
Article:
Jin, H, Lin, G, Bai, L et al. (3 more authors) (2016) Photothermal conversion efficiency of nanofluids: An experimental and numerical study. Solar Energy, 139. pp. 278-289. ISSN 0038-092X

https://doi.org/10.1016/j.solener.2016.09.021

Photothermal Conversion Efficiency of Nanofluids: An Experimental and Numerical study

Haichuan Jin[1,2] Guiping Lin[1] Lizhan Bai[1,2] Muhammad Amjad[2]
Enio Bandarra[3] Dongsheng Wen[2,*]

1 Laboratory of Fundamental Science on Ergonomics and Environmental Control, School of Aeronautic Science and Engineering, Beihang University, Beijing 100191, PR China

2 School of Chemical and Process Engineering, University of Leeds, Leeds, LS2 9JT, UK

3 Department of Mechanical Engineering, Federal State University of Uberlandia, Uberlandia, Brazil

Abstract: This work investigated experimentally the photothermal conversion efficiency (PTE) of gold nanofluids in a cylindrical tube under natural solar irradiation conditions, and compared with a developed 3-dimensional numerical model. The PTE of gold nanofluids was found to be much higher than that of pure water, and increased non-linearly with particle concentration, reaching 76% at a concentration of 5.8 ppm. Significant non-uniform temperature distribution was identified both experimentally and numerically, and a large uncertainty can be caused in the PTE calculation by using only one temperature measurement. A mathematical model was also developed to calculate the absorption efficiency without knowing the temperature field, which can be used to predict the theoretical PTE for nanofluids based on their optical properties only.

Keywords: nanoparticle; nanofluid; solar energy; photothermal conversion efficiency, direct absorption

* Corresponding author. Tel.: 0044-113-3432678; fax: 0044-20-78825003.
E-mail address: d.wen@leeds.ac.uk

Nomenclature

A	surface area exposed to solar radiation (m^2) / absorbance (-)
a_n	Mie coefficient to compute the amplitudes of the scattered field (-)
b_n	Mie coefficient to compute the amplitudes of the scattered field (-)
c	specific heat capacity ($J/(kg \cdot K)$)
c_p	specific heat capacity ($J/(kg \cdot K)$)
D	particle diameter (m)
E	spectral emissive power (W/m^3)
f_v	volume concentration (-)
h	convection coefficient ($W/(m^2 \cdot K)$)
I	radiative intensity (W/m^2)
k	thermal conductivity ($W/(m \cdot K)$)
k_f	imaginary part of the complex refractive index of the based fluid (-)
L	optical depth (m)
m	mass (kg) / relative refractive index (-)
n	complex refractive index (-) / order of accuracy
q	heat flux (W/m^2)
Q	efficiency factor for Mie scattering (-)
Q_r	radiative heat source in heat transfer equation
R	radius of cylinder experimental tube (m)
r	radius in integrating process (m)
$\hat{s}$	one specific direction which contains infinitesimal pencil of rays
T	temperature ($^{\circ}C$)
t	time (s)
u	velocity (m/s)

x	characteristic size of nanoparticles (-)
Greek symbols	
β	extinction coefficient (m^{-1})
Φ	scattering phase function
ε	spectral emissivity
η	efficiency (-)
κ	absorption coefficient (m^{-1})
λ	wavelength of light in vacuum (m)
σ	scattering coefficient (m^{-1}) / Stefan-Boltzmann constant = $5.670\times10^{-8}\left(\mathrm{W}/\left(\mathrm{m}^2\cdot\mathrm{K}^4\right)\right)$
Ω	solid angle
ρ	density
ψ_n	spherical Bessel function of order n
ξ_n	spherical Bessel function of order n
Superscripts	
-	average value
$\rightarrow$	vector quantity
Subscripts	
abs	absorption
amb	ambient
b	black body
ext	extinction
f	fluid
η	wavelength range
i	direction number of light
n	nanoparticle
out	outlet
p	particle

sca	scattering
s	scattering
w	water

1 Introduction

The concerns over excessive use of fossil energies and increasing environmental problems have accelerated rapid development of solar energy technologies [1]. However, the difficulties in efficiently collecting solar energy and converting it into useful energies (i.e., either electricity or heat) limit the extensive utilization of solar energy [2]. Most of solar thermal collectors have 'tube-in-plate' arrangements, which absorb solar energy on their surfaces and transfer heat to a working fluid running inside the tubes. Such an arrangement is surface-limited, i.e., relying on the transfer of heat from a tube surface to the fluid inside. This would produce a large temperature difference between the fluid and the absorber especially for high temperature applications (i.e., solar thermal power plants) [3], and result in a limited solar energy utilization efficiency.

The concept of volumetric solar energy absorption, i.e., certain materials are seeded in a working fluid to absorb solar energy directly within the fluid itself, was originated in 1970's and coined as direct absorption solar collector (DASC) [4]. In the concept, selective tube materials are used to allow most of the solar energy pass through the wall and into the fluid, but prevent the radiation leakage from the fluid, forming a 'thermal trapping' phenomenon[5]. In this way, the highest temperature exists in the fluid and the overall conversion efficiency from solar energy to heat can be largely improved due to reduced re-radiation heat loss.

The use of nanoparticles as effective absorption media is a recent development. It has been reported that adding very diluted particles into base fluid could enhance the radiative absorbing efficiency and improve the overall heat transfer rate due to their large specific surface areas [6]. A range of nanoparticles including metal (such as Cu, Au, and Ag), metal oxide (such as TiO_2, Al_2O_3) and carbon materials [7–11] have been investigated under laboratory [3,12–14] and natural sunlight conditions [15–17]. Some results were very encouraging. For instance, the solar conversion efficiency of a 0.01% graphite nanofluid was found to be as high as 122.7% of that of a conventional surface absorbing collector [12]. Some metallic nanoparticles such as gold and silver have also drawn wide attentions because of their Surface Plasmon Resonance effects (SPR)

[18,19]. For these kinds of materials, the resonance frequencies of conduction electrons are usually in the visible-light spectrum , which is weakly absorbed by most of the heat transfer fluids but occupies nearly half of the total solar radiation energy [20]. Zhang et al. [14] showed that a very low concentration of gold nanoparticles (i.e., mass concentration of 0.0028%) could increase the photothermal conversion efficiency (PTE) of the base fluid by 20%, reaching an impressive specific absorption rate (SAR) of ~10 kW/g under laboratory conditions. In another study conducted outdoor, up to 144% enhancement in the stored thermal energy was obtained for 6.5 ppm silver nanoparticle-based direct absorption under natural sunlight conditions [15]. However it shall be noted that only one temperature was measured in most of the published work [21–25] and a uniform temperature assumption was used to calculate the energy efficiency, neglecting the temperature distribution within the fluid. Considering a reduced radiative intensity along the path of the absorbing liquid, there shall exist large temperature non-uniformity in the fluid, whose neglect may lead to inaccurate calculations for the PTE and disguise some key parameters (such as the optical depth) in optimizing the collector design.

Quite a few studies [3,24,26–28] have built numerical models to simulate the radiative and heat transfer process in nanofluids. Unfortunately, most of these simulative studies were based on the ideal solar spectrum, and ignored that the spectral emissive power distribution is affected by the atmosphere's absorption, especially in the infrared spectrum. As the radiation properties of nanoparticles are highly spectral dependent, any numerical work should consider the solar spectrum associated with realistic experimental conditions. A theoretical method to predict photothermal efficiency directly based on nanoparticle's basic physical properties with respect to particle loadings and optical depth has yet to be established.

To overcome the issues reviewed above, a detailed investigation of the photothermal conversion characteristics of gold nanoparticle dispersions was conducted both experimentally and numerically. Gold nanoparticles were synthesized via a one-pot reaction, and the experiments were performed under natural

sunlight conditions with multiple temperature measurement. A 3-dimensional model was developed to simulate the experimental results, which was followed by a parametric investigation of the influence of particle concentration, solar radiation intensity and receiver geometrical parameters on the solar conversion efficiency. A new method to theoretically predict the photothermal conversion efficiency of nanoparticle dispersions was proposed according to the radiative transfer equation.

2 Experimental investigation

2.1 Gold nanoparticle dispersions formulation

In this study, a one-step method [29] was used to produce gold nanoparticle dispersions and different concentrations were prepared. A typical procedure is introduced below as an illustration, i.e., CASE 6 in **Table 1**. Here 2.5×10^{-7} mol $HAuCl_4$ was dispersed into 50 ml DI water in a three-necked flask under heating. A magnetic blender was used to stir the liquid until boiling. Boiling was continued for 10 min and then 50 ml of 1×10^{-5} mol/L sodium citrate was added. The solution turned dark blue within 30 seconds and the final color became wine red after being heated for an additional 20 minutes. The size and shape of CASE 6 identified by a transmission electron microscopy are shown in **Fig. 1a**. **Table. 1** represents 6 cases of gold nanoparticle dispersions. The dispersions were maintained good stability for over two months, and were used for the below experiments without further purification and separation.

An UV/Vis spectrometer (UV-1800 SHIMADZU UV Spectrophotometer) was applied to measure the absorption spectrum of the nanoparticle dispersions at different concentrations. As shown in **Fig. 1b**, due to the strong surface Plasmon resonance of gold nanoparticles in the visible light spectrum[14], a peak absorption wavelength was found at 526 nm for all the dispersions, which is consistent with the TEM analysis that the size of gold nanofluids was about 20 nm. According to the Beer-Lambert Law (known as Beer's Law) [30], also seen in Eq. 8 below, there is a linear relationship between the absorbance and the concentration of the sample, as shown in the inset.

2.2 Experimental settings

The experimental setup in this study is showed in **Fig. 2a** and **b**. The tubes used in this experiment were custom-made from high temperature resistant quartz glass. The tube contained a vacuum interlayer to reduce the impact of convection from outside air. The sample fluids were placed in the inside-tube with a diameter of 25 mm and length of 300 mm. The outside-tube had a diameter of 60 mm with two small-bore pipes, which were used to fix temperature sensors.

As shown in **Fig. 2b**, three T-type thermocouples (Omega TT-T-40-SLE) with a precision of ±0.5 K were placed evenly in the bottom, middle, top of the sample fluids along the optical depth, and two more thermocouples were applied to measure the air inside and outside the tube (i.e., the ambient), respectively. A data acquisition (Agilent 34970A) system was used to measure the thermocouple voltage signal and then transferred it into digital form, recorded in a PC under LabVIEW environment. A solar radiation intensity sensor was employed to measure the solar intensity, and the data was also recorded in the PC.

3 Experimental results analysis

3.1 Temperature variation

Example temperature curves of gold nanofluids and DI water under varied natural solar intensity are shown in **Fig. 3a**, together with the air temperature inside and outside the tube. A slow increase in DI water temperature is observed and the solar intensity (I) was varied from about 400 W/m^2 to 700 W/m^2. Clearly the temperature variation of both water and nanofluids lags behind, but gold nanofluids show much more rapid temperature increase under the same intensity than pure water. For example, the bulk temperature is increased by ~21 K after 60 minutes' heating for a GNP concentration of 5.8 ppm, more than three times of pure water temperature rise. Here the average temperature from three thermocouples, i.e., ($\overline{T} = \left(T_{TC1} + T_{TC2} + T_{TC3}\right)/3$), was used to represent the fluid temperature.

To reveal the possible temperature difference inside the fluid, **Fig. 3b** shows the temperature profiles of

three thermocouples for 5.8 ppm gold nanofluid and DI water respectively under the same condition as Fig. 3a. . Consistent large temperature difference was found for the nanofluid. A maximum 2.6 K temperature difference was found for nanofluid after 28 minutes' illumination, but for DI water, the maximum temperature difference was in a relative small region (i.e., less than 0.5 K). Considering the potential large temperature difference in the nanofluid, as will be revealed by the numerical model, the location of the thermocouple would affect the calculated PTE significantly if only one measurement was used.

Fig. 3c shows an example of the influence of solar intensity variation on the PTE for 0.72 ppm gold nanofluid. For the constant solar intensity case , the temperature increased smoothly and reached the equilibrium point after two hours' illumination; but for varied solar intensity (cloudy day), the same nanofluid exhibits a changing tendency, which follows the pattern of solar intensity variation. Generally, salient temperature difference among three thermocouples can be observed under both solar intensities, being larger for a higher solar intensity. Further non-uniform temperature distribution and its effects on the solar efficiency is discussed in **section 5**.

3.2 Efficiency and SAR

The average photothermal conversion efficiency (PTE) is defined as the ratio of the internal energy increase of the fluid to the total incoming radiation input:

$$\eta = \frac{(c_w m_w + c_n m_n)\Delta T}{IA\Delta t} \approx \frac{c_w m_w}{IA} \cdot \frac{\Delta \bar{T}}{\Delta t} \qquad (1)$$

where $\Delta \bar{T}$ is the average temperature difference ($\Delta \bar{T} = (\Delta T_{TC1} + \Delta T_{TC2} + \Delta T_{TC3})/3$). Comparing with the base water, thermal energy stored in gold nanoparticles is negligible owing to extremely low concentration: i.e., a maximum of 5.8 ppm in volume (0.01% in mass).

To quantify the capability of nanoparticles in absorbing solar energy, the specific absorption rate (SAR) is employed[15]:

$$SAR = \frac{\left(c_w m_w + c_n m_n\right)\Delta \bar{T}_n - c_w m_w \Delta \bar{T}_w}{m_n \Delta t} \quad (2)$$

The calculated PTEs within the measurement uncertainty of $\pm 3\%$ under two different solar intensities are shown in **Fig. 4**, which is in general similar to previous studies[14,15]. The PTE reaches 45.5% even at a relatively low concentration (0.36 ppm), increased by 163% comparing with the base water (17.3% at $I = 950 W/m^2$). The highest PTE of gold nanofluids is 73.6%, which is more than 4 times of DI water and more promising than what found in previous studies [12,14,31]. The PTE increases rapidly under low particle concentrations and approaches asymptotically to a constant value when the concentration reaches a certain status (i.e., 1 ppm for $I=600\ W/m^2$). A lower PTE value (i.e., 10% smaller) is found for the high solar intensity case, which is assumed to be related to an increased heat loss. **Fig. 4** also shows that SAR rapidly decreases with the increasing concentration below 1 ppm, and the highest SAR reaches $2.715\ kW/g$ at nanoparticle concentration of 0.36 ppm for $I=950\ W/m^2$ solar intensity, which is in the broad range of previous studies [14,15]. Further investigation with numerical results will be conducted regarding to PTE and SAR in **section 5.**

4 Numerical model of direct absorbing solar energy for nanofluids

4.1 Solar radiation and Mie scattering theory

In order to get better understanding of radiative heat transfer in gold nanofluids, a numerical model was built in this work. Realistic solar irradiation profile was calculated based on ASTM G173-03 Reference Spectra [32]. As shown in **Fig. 5a**, the solar irradiation on the ground is distinctly different from that at top of atmosphere, especially for spectral emissive power in infrared, which is due to the intense absorption of H_2O and CO_2 in atmosphere. The result from integrating the spectral emissive power with wavelength shows that nearly 99% of solar radiation energy at sea level exists in 0.2~3 μm. As solar emissive power takes part of nearly 43% in infrared, which can be seen in the inset figure, considering the actual solar spectrum on the ground becomes essential for solar thermal applications. For the purpose of proper simplification [3], spectral emissive power

for sun (T=5762 K) and nanofluid (T=303 K) has been calculated and separated into two bands on wavelength of $3\,\mu m$ (see in **Fig. 5b**); Solar irradiation wavelength locates mainly below $3\,\mu m$ with a peak at 480 nm, while wavelength for nanofluid of 303 K is beyond $3\,\mu m$.

In the present modeling, the characteristic size employed in radiative transfer equation is as $x_\lambda = \pi D / \lambda$, where D represents the diameter of nanoparticles. For our experimental study, the diameter of gold nanoparticles is 20 nm characterized by TEM as shown in **Fig. 1a**. Although it is appropriate to use simplified equations, i.e., the Rayleigh scattering approximation [30], to calculate the absorption coefficient, since the diameter of suspended particles in the experiments are much smaller than the wavelength of irradiation (x_λ <<1). The original Mie scattering equations [30] is preferred to identify the optical properties for spherical nanoparticle suspensions in order to obtain detailed scattering parameters, such as the efficiencies for scattering, absorption, backscattering, averaged absolute-square E-field. The Mie scattering equations can be described by:

$$a_n = \frac{m\psi_n(mx)\psi_n'(x) - \psi_n(x)\psi_n'(mx)}{m\psi_n(mx)\xi_n'(x) - \xi_n(x)\psi_n'(mx)} \tag{2-a}$$

$$b_n = \frac{\psi_n(mx)\psi_n'(x) - m\psi_n(x)\psi_n'(mx)}{\psi_n(mx)\xi_n'(x) - m\xi_n(x)\psi_n'(mx)} \tag{2-b}$$

$$Q_{sca}(\lambda) = \frac{2}{x^2}\sum_{n=1}^{\infty}(2n+1)\left[|a_n|^2 + |b_n|^2\right] \tag{2-c}$$

$$Q_{ext}(\lambda) = \frac{2}{x^2}\sum_{n=1}^{\infty}(2n+1)\,\mathrm{Re}(a_n + b_n) \tag{2-d}$$

where the functions $\psi_n(x)$ and $\xi_n(x)$ are spherical Bessel functions[30] of order n (n= 1, 2,..) and the primes refer to the derivatives with respect to the argument, and m represents the ratio of refractive indexes, calculated by:

$$m = \frac{n_{particles}}{n_{fluid}} \tag{3}$$

where $n_{particles}$ and n_{fluid} are the complex refractive index [33–35] of gold and based fluid relative to the ambient medium, respectively. In consideration of relative low concentrations of nanofluids developed for solar thermal applications, particles should absorb and scatter light independently according to the scattering map [30]. With such a consideration, the absorption coefficient can be calculated from the below equation:

$$\kappa(\lambda)=\kappa_{p}(\lambda)+\kappa_{f}(\lambda)=\frac{3\pi}{2}\frac{f_{v}Q_{abs}(\lambda)}{D}+\frac{4\pi k_{f}(\lambda)}{\lambda} \quad (4)$$

4.2 Radiative transfer equation and heat transfer equation

The property of spectral intensity can be described simultaneously by the radiative transfer equation, known as RTE [30]:

$$\hat{s}\cdot\nabla I_{\eta}=\kappa_{\eta}I_{b\eta}-\beta_{\eta}I_{\eta}+\frac{\sigma_{s\eta}}{4\pi}\int_{4\pi}I_{\eta}(\hat{s}_{i})\Phi_{\eta}(\hat{s}_{i},\hat{s})d\Omega_{i} \quad (5\text{-a})$$

$$\nabla\cdot q_{\eta}=\kappa_{\eta}\left(4\pi I_{b\eta}-\int_{4\pi}I_{\eta}d\Omega\right) \quad (5\text{-b})$$

$$\kappa_{\eta}=\beta_{\eta}-\sigma_{s\eta} \quad (5\text{-c})$$

where I_{η} represents the radiative intensity of wavelength range $\lambda_{\eta_1}\rightarrow\lambda_{\eta_2}$ in the direction $\hat{s}_{i}$, $I_{b\eta}$ is the re-emission of nanofluid, $\Phi_{\eta}(\hat{s}_{i},\hat{s})$ is called the scattering phase function and describes the probability that a ray from one direction $\hat{s}_{i}$, will be scattered into a certain other direction $\hat{s}$, κ_{η}, β_{η} and σ_{η} are the absorption, extinction and scattering coefficient, respectively. Spectral radiative heat flux q_{η} can be obtained by integrating the radiative intensity with the solid angle Ω .

Transient heat transfer equation is shown as:

$$\rho c_{p}\frac{\partial T}{\partial t}+\rho c_{p}\vec{u}\cdot\nabla T+\nabla\cdot\vec{q}=Q_{r} \quad (6\text{-a})$$

$$\vec{q}=-k\nabla T \quad (6\text{-b})$$

$$Q_{r}=-\int_{0}^{\infty}q_{\eta}(\lambda)d\lambda \quad (6\text{-c})$$

The boundary condition and initial condition are:

$$-\vec{n}\cdot\vec{q}=\varepsilon\sigma\left(T^{4}_{amb}-T^{4}\right)+h\left(T_{amb}-T\right)\Big|_{contact\_air} \quad (7\text{-a})$$

$$T_{t=0} = T_i \tag{7-b}$$

where h is the convection coefficient due to convection from one end of the tube contacted with air outside, whose contribution to the result is small and a typical value of $15\ W/(m^2 \cdot K)$ is used in this work.

4.3 Predicted absorption efficiency for nanofluids

For most of our applied particles, scattering contribution can be neglected according to the Mie theory. Furthermore, the radiative equations can be simplified as a 1-dimentional transfer process. Under these assumptions, an analytical solution for Eq. (6-a) can be obtained:

$$E_\lambda(L) = E_{\lambda,(y=0)} e^{-\beta_\lambda L} + E_{bb,\lambda}(1 - e^{-\beta_\lambda L}) \tag{8}$$

where E represents the spectral emissive power with unit of W/m^3. In order to investigate the spectrum behavior at wavelength below $1.1\ \mu m$, which is the upper limit of our spectrophotometer, black body re-emissive radiation can be neglected due to the small intensity of re-emission, seen in **Fig. 5b**. Coupled with Eq. 5, Eq. 9 can be further simplified as:

$$-\log\left(\frac{E_{out}(\lambda)}{E_0(\lambda)}\right) = \beta_\lambda \cdot L \cdot \log_{10} e = \left(\frac{3\pi}{2}\frac{Q_{abs}(\lambda)}{D} \cdot \log_{10} e\right) \cdot f_v \cdot L = A(\lambda) \tag{9}$$

Eq.10 represents the analytic derivation process of the famous Beer-Lambert Law [30]. With these assumptions, a new method is proposed to evaluate the total absorption efficiency (ABE) for a given nanoparticle concentration and optical depth, which is the theoretical maximum possible photothermal conversion efficiency:

$$\eta(L, f_v) = \frac{\int_{0.2\mu m}^{3\mu m} E_0(\lambda)\left(1 - 10^{-A(\lambda)\frac{L}{L_0}}\right) d\lambda}{\int_{0.2\mu m}^{3\mu m} E_0(\lambda) d\lambda} = \frac{\int_{0.2\mu m}^{3\mu m} E_0(\lambda)\left(1 - e^{-\kappa(\lambda,\ f_v)L}\right) d\lambda}{\int_{0.2\mu m}^{3\mu m} E_0(\lambda) d\lambda} \tag{10}$$

Further investigation will be discussed in next section with experimental results.

4.4 Solution methodology

A high-order algorithm has been used to solve Eqs. (3) ~ (5) and (11) to calculate coefficients related to

optical properties for nanofluids and photothermal conversion efficiency, with functions powered by Matlab associated with COMSOL Multiphysics, similar to the one described by Kluczyk[36]. It should be noticed that obtaining an analytical solution to Eqs. (6) ~ (8) is extremely difficult as the 3-dimentional transient heat transfer equations coupled with transient RTE equations are complicated partial differential equations. A finite element method (FEM) was employed to solve the equations numerically in COMSOL. A predefined Heat Transfer with Radiation in Participating Media equations [30] together with user defined functions (radiative transfer equation) were used to describe thermal and radiative energy transfer process. The discretization of the simulative space was conducted with the appliance of a built-in non-structured meshing COMSOL algorithm. The maximum element size inside nanofluid was chosen as 0.2 cm, and the maximum was chosen as 0.05 cm for the surface with respect to radiative and convective heat loss, which mainly happens at the surface. A direct solver called MUltifrontal Massively Parallel sparse direct Solver (MUMPS) with tolerance of 10^{-5} was adopted to numerically solve the matrices assembled according to the governing equations and boundary conditions described above. The initial and boundary conditions were originated from experimental measurement (such as temperature of inside air and the ambient). With Mie scattering, RTE, transient heat transfer equations coupled with varying boundary conditions, it is very demanding on the computational power. The Advanced Research Computing (ARC) at University of Leeds is used to solve the equations in in parallel.

5. Numerical results and comparison

5.1 Validation against experimental data

The absorption coefficients for gold nanoparticles and working fluid (water) calculated by Mie scattering theory (Eqs.3-5) can be seen in **Fig. 6a,** where the volume concentration of gold particles is 5.8 ppm. The absorption coefficient which cannot be obtained through experiments is a key parameter for 3D heat transfer and radiative transfer equations. As shown in **Fig. 6a**, gold nanoparticles contribute the absorption in the visible light spectrum and the base fluid (water) is more effective in the infrared range. To examine the

reliability of our calculation, the absorbance from numerical results based on Eq.10 is compared with experimental value in **Fig. 6b**. The simulation result is generally in agreement with the experimental value. The experimental deviation in 600~800 nm is due to the existence of some bigger particles in the fluids, which could make the absorbance red shift.

Based on experimental boundary and initial conditions, as an example, the comparison of the simulation with experimental results under constant solar intensity (i.e., 950 W/m^2) is shown in **Fig. 7.** The temperature rise of 1.45 ppm gold nanofluid is much higher than that of DI water, for example ~25 K for nanofluid and ~12 K for water. However, both nanofluid and water exhibit non-uniform temperature distribution during the illumination, as much as 4.4 K and 1.9 K temperature difference can be reached, respectively. The high temperature of the top layer (TC1) shows that solar energy is mostly absorbed in the surface layer. The low temperature at the bottom layer is related to effects of solar intensity decay along the optical path, and the limited heat conduction capacity. After about three hours' heating, nanofluid can maintain approximately an equilibrium temperature (~ 57 ℃), but for water the maximum is only ~ 45 ℃ , indicating that gold nanofluid even with very low concentration can significantly enhance the energy conversion from solar radiation to thermal form.

5.2 Temperature distribution profile inside the tube

Non-uniform temperature distribution can be further demonstrated through T-profile in 3-dimensional fluid (gold nanoparticles with volume concentration of 1.45 ppm, water as based fluid, under constant solar intensity, i.e., 950 W/m^2), which can be seen in **Fig. 8a**. The result in this case shows that the temperature at the up middle of the tube along Y direction is higher than the bulk value. Generally, the highest temperature is located inside the nanofluid volume (about 0.8 cm to the illuminated surface), for example 44 ℃ in this case. Clearly larger temperature difference (i.e., more than 6 K) for the whole considered volume can be seen in **Fig. 8b**, comparing with the 3 thermocouple measurement in **Fig. 7**, which illustrates the danger of using individual

335 measured values to calculate PTE.

336 **5.3 Efficiency prediction and comparison**

337 Most of the prior studies such as Andrej et al. [3] were based on experimental or simulative temperature
338 field to optimize the efficiency of nanofluid-based DASC. Here we report a mathematical method to predict
339 the absorption efficiency (ABE), which represents the maximum possible efficiency for any nanofluid-based
340 solar system, according to optical properties, seen in Eq. (11).

341 **Fig. 9a** shows the absorption efficient in different wavelength. Clearly comparing to the water case, much
342 higher ABE is observed for gold nanofuids across the whole solar spectrum. The spectrum ABE increases with
343 the particle concentration, and nearly 100% ABE is achieved for 5.8 ppm nanofluids in the visible light
344 spectrum, which is related to the surface plasmon resonance phenomenon of gold nanoparticles. The small
345 depression at ~900 nm is associated with the poor absorbency performance in the near-infrared, which can
346 be explained by the Mie scattering theory.

347 **Fig. 9b** and **c** show the ABE as a function of optical length L and particle concentration f_v. The initial
348 efficiency of the nanofluids receiver increases rapidly with L, then asymptotically reaches 100%. This result is
349 similar to Zhang et al.[14]'s experimental observation, where it showed clearly that the PTE increased
350 nonlinearly with volume concentration but no proper explanation was provided. As shown in radiative transfer
351 equations (Eq. 9), the radiative transport energy is consumed inside nanofluid exponentially, and the PTE
352 should exhibit a nonlinear dependence on the particle concentration.

353 **Fig. 9** also reveals the important parameters that determine the maximum possible solar receiver efficiency.
354 The impact of the optical depth L and particle concentration f_v is embedded in the exponential term as
355 $L \cdot f_v$ in Eq. 9. **Fig. 9b** reveals that both optical concentration and optical depth should be in a relative small
356 values to achieve an optimized effect, as higher volume concentration of nanoparticle (i.e., more than 10 ppm
357 for L=0.05 m) increases the efficiency slightly. Comparing to nanofluids, the efficiency depends more on the

optical depth to reach a relative high value (i.e., 25 m for 80%). Overall, employing GNPs enhances the ABE significantly compared with pure water.

In order to compare the prediction of ABE against experimental and simulative data (i.e., where the optical depth is not a constant), a modified equation is proposed by integrating the efficiency with the radius, as:

$$\eta\left(\mathrm{f_v}\right)=\frac{\int_0^{\mathrm{R}}\int_{0.2\mu\mathrm{m}}^{3\mu\mathrm{m}}\mathrm{E_0}\left(\lambda\right)\left(1-\mathrm{e}^{-2\kappa\left(\lambda,\,\mathrm{f_v}\right)\mathrm{r}}\right)\mathrm{d}\lambda\mathrm{dr}}{\mathrm{R}\int_{0.2\mu\mathrm{m}}^{3\mu\mathrm{m}}\mathrm{E_0}\left(\lambda\right)\mathrm{d}\lambda} \tag{11}$$

where R is the radius of cylindrical tube. The ABE becomes an only function of volume concentration. The ABE is compared with three ways of photothermal conversion efficiencies based on temperature field, i) from one measured thermocouple, ii) from the average temperature measured by three thermocouples, and iii) from the simulated temperature field. For the simulated data, the efficiency is obtained by considering temperature difference in each computational nodes, as:

$$\eta=\frac{\sum_{\mathrm{i=1}}^{\mathrm{n}}\mathrm{c_w}\rho_{\mathrm{w}}\mathrm{V_i}\Delta\mathrm{T_i}}{\mathrm{IA}\Delta\mathrm{t}} \tag{12}$$

Fig. 10a shows reasonably good agreement from four different methods. It can be expected that ABE from Eq. 12 is the theoretical maximum efficiency, in which the scattering and heat leakage are not considered. It can be used as an efficient method for nanoparticle selection and solar collector optimization without the need of measuring the temperature field. Photothermal efficiency based only on one temperature point shows a large underestimation of the PTE for all samples. For example, the PTE is 12% lower than that from the experiment-determined average temperature at f_v=5.8 ppm.

What's more, the temperature used to determine PTE is usually at the beginning when the heat leak is not significant, the temperature difference (i.e., 4.4 ℃ for 1.45 ppm under 950 W/m^2 solar intensity) inside nanofluid is comparable to this temperature range (10-15 ℃). Neglecting of non-uniform temperature distribution could cause significant inaccuracy (with an uncertainty of 29%-44%) in calculating the energy

efficiency. To illustrate such an effect, **Fig. 10b** shows the maximum differences in temperature and PTE based on the simulation result under a solar intensity of 1000 W/m^2 and particle size of 20 nm. Here the temperature elevation employed to determine PTE is 10 K from the beginning of the experiment. Depending on the measurement location, as high as 67% uncertainty could be obtained for the case of 5.8 ppm gold nanofluid.

The temperature non-uniformity issue will become more and more serious when the volume concentration of nanofluids increases or the radiation intensity increases (i.e., under focused solar intensities). Quite a few recent studies [13,16,17,37] have shown that under a focused solar light, i.e., via a typical Fresnel lens, rapid steam can be produced from plasmonic nanofluids albeit the bulk solution was still under subcooled conditions. In one study [16], by using very dilute gold nanoparticles (16.7 ppm) under a solar concentration of 1000 times, , steam generation efficiency was calculated as high as 80%, and only 20% of the absorbed solar energy was used to increase the bulk fluid temperature. However, there is still a strong debate if the steam can be produced around heated nanoparticles. Considering the potential large temperature difference in the fluids under a focused solar intensity, there is a possibility that steam could be produced on the strongly heated surface layer, where strong evaporation or even boiling can occur. Further exploration of this issue is ongoing, and will be presented in the future.

6 Conclusions

Both outdoor experiments and simulation were conducted in this work to analyses the photothermal conversion characteristics of gold nanofluids, and a new method was proposed to predict the theoretical efficiency based only the optical properties. The main conclusions can be summarized as:

(1) The photothermal conversion efficiency of gold nanofluids is much higher than that of pure water, and increased non-linearly with particle concentration, reaching 76% at a concentration of 5.8 ppm.

(2) Significant non-uniform temperature distribution was identified inside the fluid, indicating that the consideration of average temperature is needed to obtain a reliable PTE.

(3) A new method was developed to predict radiative absorption efficiency based on the optical properties of nanofluid, without the need of knowing the temperature field inside the fluid. The method can be used to identify the performance of nanoparticles and optimize solar absorbers efficiently.

(4) A radiative heat transfer model coupled with the Mie scattering theory was developed. This model can predict temperature profile successfully, which confirms the existence of large temperature difference inside nanofluids.

(5) The comparison of various efficiencies shows that Eq. (11) can be used to predict the theoretical maximum photothermal conversion efficiency, and using only one-point temperature measurement could cause significant inaccuracy, i.e., uncertainty of 67% for 12.75 ppm gold nanofluid at 1000 W/m^2 solar intensity.

ACKNOWLEDGEMENT

This work was supported by the EU Marie Curie Actions-International Incoming Fellowships (FP7-PEOPLE-2013-IIF-626576), and the author Haichuan Jin also acknowledges the financial support for his visiting study at the University of Leeds from the China Scholarship Council (CSC) under the Grant No.201506020031.

References

[1] Sukhatme SP. Solar thermal power generation. J Chem Sci 1997;109:521–31. doi:10.1007/BF02869211.

[2] Gupta HK, Agrawal G Das, Mathur J. An experimental investigation of a low temperature Al2O3-H2O nanofluid based direct absorption solar collector. Sol Energy 2015;118:390–6. doi:10.1016/j.solener.2015.04.041.

[3] Lenert A, Wang EN. Optimization of nanofluid volumetric receivers for solar thermal energy conversion. Sol Energy 2012;86:253–65. doi:10.1016/j.solener.2011.09.029.

[4] Minardi JE, Chuang HN. Performance of a “black” liquid flat-plate solar collector. Sol Energy 1975;17:179–83. doi:10.1016/0038-092X(75)90057-2.

[5] Arai N, Itaya Y, Hasatani M. Development of a “volume heat-trap” type solar collector using a fine-particle semitransparent liquid suspension (FPSS) as a heat vehicle and heat storage medium Unsteady, one-dimensional heat transfer in a horizontal FPSS layer heated by thermal radiatio. Sol Energy 1984;32:49–56. doi:10.1016/0038-092X(84)90048-3.

[6] Rahman MM, Al-Mazroui W a., Al-Hatmi FS, Al-Lawatia M a., Eltayeb I a. The role of a convective surface in models of the radiative heat transfer in nanofluids. Nucl Eng Des 2014;275:382–92. doi:10.1016/j.nucengdes.2014.05.028.

[7] Gan Y, Qiao L. Radiation-enhanced evaporation of ethanol fuel containing suspended metal nanoparticles. Int J Heat Mass Transf 2012;55:5777–82. doi:10.1016/j.ijheatmasstransfer.2012.05.074.

[8] Hussain I, Graham S, Wang Z, Tan B, Sherrington DC, Rannard SP, et al. Size-controlled synthesis of near-monodisperse gold nanoparticles in the 1-4 nm range using polymeric stabilizers. J Am Chem Soc 2005;127:16398–9. doi:10.1021/ja055321v.

[9] Hwang SH, Yun J, Jang J. Multi-Shell Porous TiO 2 HollowNanoparticles for

Enhanced Light Harvesting in Dye-sensitized Solar Cells. Adv Funct Mater 2014;24:7619–26. doi:10.1002/adfm.201401915.

[10] Mock JJ, Barbic M, Smith DR, Schultz D a., Schultz S. Shape effects in plasmon resonance of individual colloidal silver nanoparticles. J Chem Phys 2002;116:6755–9. doi:10.1063/1.1462610.

[11] Otanicar TP, Phelan PE, Prasher RS, Rosengarten G, Taylor R a. Nanofluid-based direct absorption solar collector. J Renew Sustain Energy 2010;2. doi:10.1063/1.3429737.

[12] Luo Z, Wang C, Wei W, Xiao G, Ni M. Performance improvement of a nanofluid solar collector based on direct absorption collection (DAC) concepts. Int J Heat Mass Transf 2014;75:262–71. doi:10.1016/j.ijheatmasstransfer.2014.03.072.

[13] Ni G, Miljkovic N, Ghasemi H, Huang X, Boriskina S V, Lin C. Volumetric solar heating of nano fl uids for direct vapor generation 2015.

[14] Zhang H, Chen HJ, Du X, Wen D. Photothermal conversion characteristics of gold nanoparticle dispersions. Sol Energy 2014;100:141–7. doi:10.1016/j.solener.2013.12.004.

[15] Bandarra Filho EP, Mendoza OSH, Beicker CLL, Menezes A, Wen D. Experimental investigation of a silver nanoparticle-based direct absorption solar thermal system. Energy Convers Manag 2014;84:261–7. doi:10.1016/j.enconman.2014.04.009.

[16] Neumann O, Urban AS, Day J, Lal S, Nordlander P, Halas NJ. Solar vapor generation enabled by nanoparticles. ACS Nano 2013;7:42–9. doi:10.1021/nn304948h.

[17] Neumann O, Feronti C, Neumann AD, Dong A, Schell K, Lu B, et al. Compact solar autoclave based on steam generation using broadband light-harvesting nanoparticles. Proc Natl Acad Sci U S A 2013;110:11677–81. doi:10.1073/pnas.1310131110.

[18] Pérez-Juste J, Pastoriza-Santos I, Liz-Marzán LM, Mulvaney P. Gold nanorods: Synthesis, characterization and applications. Coord Chem Rev 2005;249:1870–901.

463 doi:10.1016/j.ccr.2005.01.030.

464 [19] Eustis S, el-Sayed M a. Why gold nanoparticles are more precious than pretty gold: noble metal surface
465 plasmon resonance and its enhancement of the radiative and nonradiative properties of nanocrystals of
466 different shapes. Chem Soc Rev 2006;35:209–17. doi:10.1039/b514191e.

467 [20] Thuillier G, Hersé M, Labs D, Foujols T, Peetermans W, Gillotay D, et al. The solar spectral irradiance
468 from 200 to 2400 nm as measured by the SOLSPEC spectrometer from the ATLAS and EURECA
469 missions. Sol Phys 2003;214:1–22. doi:10.1023/A:1024048429145.

470 [21] He Q, Wang S, Zeng S, Zheng Z. Experimental investigation on photothermal properties of nanofluids
471 for direct absorption solar thermal energy systems. Energy Convers Manag 2013;73:150–7.
472 doi:10.1016/j.enconman.2013.04.019.

473 [22] Kasaeian A, Daviran S, Azarian RD, Rashidi A. Performance evaluation and nanofluid using capability
474 study of a solar parabolic trough collector. Energy Convers Manag 2015;89:368–75.
475 doi:10.1016/j.enconman.2014.09.056.

476 [23] Ladjevardi SM, Asnaghi A, Izadkhast PS, Kashani AH. Applicability of graphite nanofluids in direct
477 solar energy absorption. Sol Energy 2013;94:327–34. doi:10.1016/j.solener.2013.05.012.

478 [24] Tyagi H, Phelan P, Prasher R. Predicted Efficiency of a Low-Temperature Nanofluid-Based Direct
479 Absorption Solar Collector. J Sol Energy Eng 2009;131:041004. doi:10.1115/1.3197562.

480 [25] Yousefi T, Veysi F, Shojaeizadeh E, Zinadini S. An experimental investigation on the effect of
481 Al2O3–H2O nanofluid on the efficiency of flat-plate solar collectors. Renew Energy 2012;39:293–8.
482 doi:10.1016/j.renene.2011.08.056.

483 [26] Hordy N, Rabilloud D, Meunier J-L, Coulombe S. High temperature and long-term stability of carbon
484 nanotube nanofluids for direct absorption solar thermal collectors. Sol Energy 2014;105:82–90.
485 doi:10.1016/j.solener.2014.03.013.

[27] Kabeel a. E, El-Said EMS. Applicability of flashing desalination technique for small scale needs using a novel integrated system coupled with nanofluid-based solar collector. Desalination 2014;333:10–22. doi:10.1016/j.desal.2013.11.021.

[28] Khullar V, Tyagi H, Hordy N, Otanicar TP, Hewakuruppu Y, Modi P, et al. Harvesting solar thermal energy through nanofluid-based volumetric absorption systems. Int J Heat Mass Transf 2014;77:377–84. doi:10.1016/j.ijheatmasstransfer.2014.05.023.

[29] Chen H-J, Wen D. Ultrasonic-aided fabrication of gold nanofluids. Nanoscale Res Lett 2011;6:198. doi:10.1186/1556-276X-6-198.

[30] Modest MF. Radiative Heat Transfer. vol. 1. Academic Press; 2003. doi:http://dx.doi.org/10.1016/B978-012503163-9/50021-7.

[31] Parvin S, Nasrin R, Alim M a. Heat transfer and entropy generation through nanofluid filled direct absorption solar collector. Int J Heat Mass Transf 2014;71:386–95. doi:10.1016/j.ijheatmasstransfer.2013.12.043.

[32] Gueymard CA. The sun's total and spectral irradiance for solar energy applications and solar radiation models. Sol Energy 2004;76:423–53. doi:10.1016/j.solener.2003.08.039.

[33] McPeak KM, Jayanti S V, Kress SJP, Meyer S, Iotti S, Rossinelli A, et al. Plasmonic Films Can Easily Be Better: Rules and Recipes. ACS Photonics 2015;2:326–33. doi:10.1021/ph5004237.

[34] Babar S, Weaver JH. Optical constants of Cu, Ag, and Au revisited. Appl Opt 2015;54:477. doi:10.1364/AO.54.000477.

[35] Hale GM, Querry MR. Optical Constants of Water in the 200-nm to 200-microm Wavelength Region. Appl Opt 1973;12:555–63. doi:10.1364/AO.12.000555.

[36] Kluczyk K, Jacak W. Damping-induced size effect in surface plasmon resonance in metallic nano-particles: Comparison of RPA microscopic model with numerical finite element simulation

509 (COMSOL) and Mie approach. J Quant Spectrosc Radiat Transf 2016;168:78–88.
510 doi:10.1016/j.jqsrt.2015.08.021.
511 [37] Hogan NJ, Urban AS, Ayala-Orozco C, Pimpinelli A, Nordlander P, Halas NJ. Nanoparticles heat
512 through light localization. Nano Lett 2014;14:4640–5. doi:10.1021/nl5016975.
513

Table captions:

Table 1 Different cases of gold nanoparticles dispersions.

Figure captions:

Fig. 1. Nanoparticle characterization: (a) TEM image of gold nanoparticles (CASE 6); (b) **A:** absorbance of gold nanoparticle dispersions under different volume fraction; **B:** peak absorbance variation with concentrations in volume.

Fig. 2. Experimental setup: (a) Soar thermal illumination experiment under nature sunlight conditions (located on the roof of Human Machine and Environment Engineering Building in Beihang University in Beijing, 39° 59' 5.49" North, 116° 21' 18.70" East.); (c) A schematic illustration of experimental setup.

Fig. 3. (a) Temperature profile of differently diluted nanofluids under varied solar intensity (cloudy, solar intensity from about 400 W/m^2 to 700 W/m^2); (b) Experimentally obtained increasing temperature profile of TC1-TC3 located inside the tube, concentration of nanofluids is 5.8 ppm and solar intensity is varied. (c) Comparison of three thermocouple signals for 0.72 ppm gold nanofluid under different solar intensities: constant solar intensity (i.e., about 950 W/m^2) and varied solar intensity (i.e., from 400 W/m^2 to 700 W/m^2).

Fig. 4. Variation of photothermal conversion efficiency (η) and specific absorption rate（SAR）with volume concentration for gold nanofulids under different solar intensities.

Fig. 5. (a) ASTM G173-03 Reference Spectra from literature, inset shows the solar energy distribution along with wavelength in percentage (integrating spectral emissive power with wavelength divided by irradiation intensity). (b) Calculation of spectral emissive power for sun (T=5762 K) and nanofluid (T=303 K), where spectral distribution is separated into two bands, A (λ<3000 nm) and B ($\lambda > 3000$ nm).

Fig.6. (a) Real and imaginary parts of m (Eq. (2)) and calculated absorption coefficients for gold nanoparticles (κ_p), working fluid (κ_f) and total (κ) according to Mie scattering theory; (b) Absorbance from Eq. (10) in comparison with results from spectrophotometer.

Fig. 7. Experimentally obtained increasing temperature profile of TC1-TC3 located inside the tube, compared with numerical results from 3D model concentration of nanofluids is 1.45 ppm and solar intensity is constantly about 950 W/m^2.

Fig. 8. (a) Schematic for numerical simulation of a 3-D volumetric solar receiver based on gold nanofluid of concentration 1.45

ppm with normal nature solar radiation I=900 W/m^2, where the geometry parameters can be seen in (b), solar radiation is in -y direction; (b) Temperature profiles in cross-section for nanofluid after 30 minutes' illumination (Global Tilt) at x=0 cm.

Fig. 9. (a) Spectral efficiency which is defined as below in this paper: $\eta_\lambda(\lambda_c)=\left[\int_{0.2\mu m}^{\lambda_c} E_0(\lambda)\left(1-e^{-\kappa(\lambda)L}\right)d\lambda\right]/\left[\int_{0.2\mu m}^{\lambda_c} E_0(\lambda)d\lambda\right]$; (b) Absorption efficiency (ABE) as a function of optical length L for 5 different volume concentrations (inset: DI water); (c) ABE as a function of volume concentration f_v for 5 different optical lengths.

Fig. 10. (a) Comparison of the experimentally obtained photothermal conversion efficiency, efficiency calculated from 3D model and predicted absorption efficiency, result based on only one thermocouple; (b) Maximum efficiency uncertainty caused by non-uniform temperature distribution in nanofluids.

549 **Table 1** Different cases of gold nanoparticles dispersions

Case No.	Reagents	Reaction time	Color	Peak size
1	$HAuCl_4$: 100ml 2.4×10^{-6}mol/L Sodium Citrate: 10ml 0.034mol/L	30 min	Wine red	9nm
2	$HAuCl_4$: 100ml 2.4×10^{-6}mol/L Sodium Citrate: 5ml 0.034mol/L	30 min	Orange	15nm
3	$HAuCl_4$: 100ml 2.4×10^{-6}mol/L Sodium Citrate: 2ml 0.034mol/L	40 min	Pink	25nm
4	$HAuCl_4$: 100ml 2.4×10^{-6}mol/L Sodium Citrate: 0.7ml 0.034mol/L	60 min	Crystal violet	65nm
5	$HAuCl_4$: 100ml 2.4×10^{-6}mol/L Sodium Citrate: 0.3ml 0.034mol/L	90 min	Ash black	120nm
6	$HAuCl_4$: 50ml 5×10^{-6}mol/L Sodium Citrate: 50ml 1×10^{-5}mol/L	20 min	Amaranth	19nm

550

551

(a)

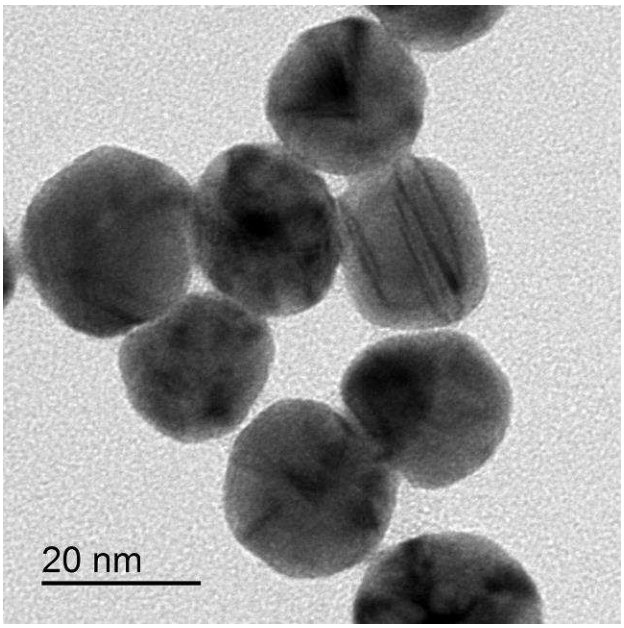

552

(b)

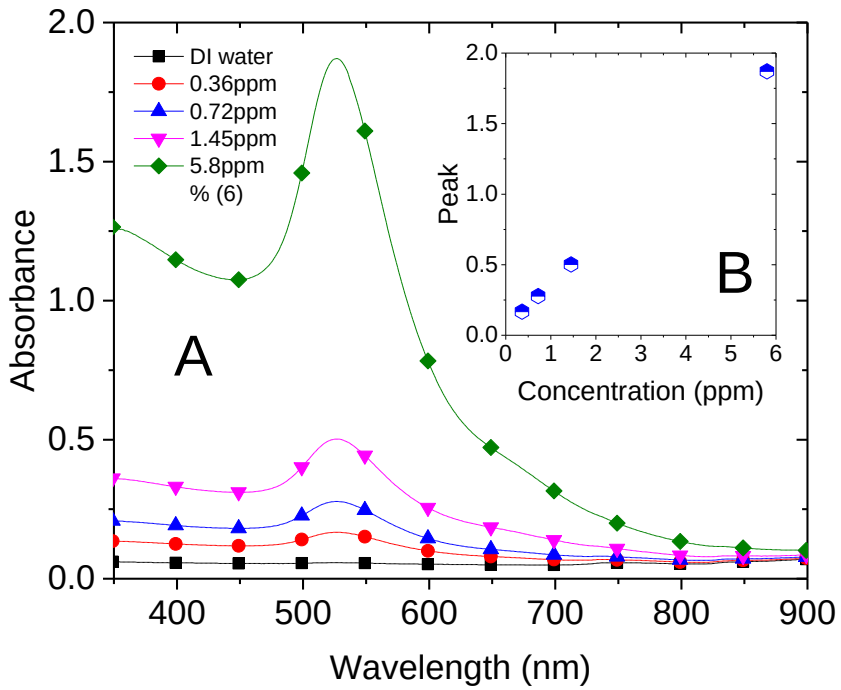

553

554 **Fig. 1.** Nanoparticle characterization: (a) TEM image of gold nanoparticles (CASE 6); (b) **A:** spectral-dependent absorbance of

555 gold nanofluid under different volume fractions; **B:** peak absorbance variation with nanoparticle concentrations.

(a)

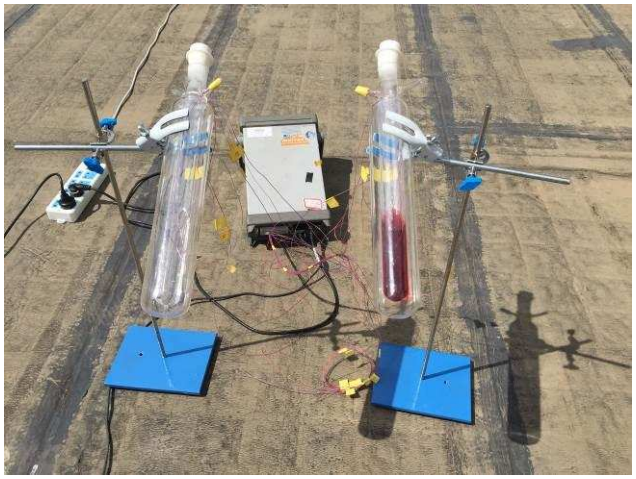

(b)

1. Thermocouples
2. Nanofluid
3. Air
4. Data acquisition
5. PC
6. Vacuum interlayer
7. Solar radiative inensity sensor

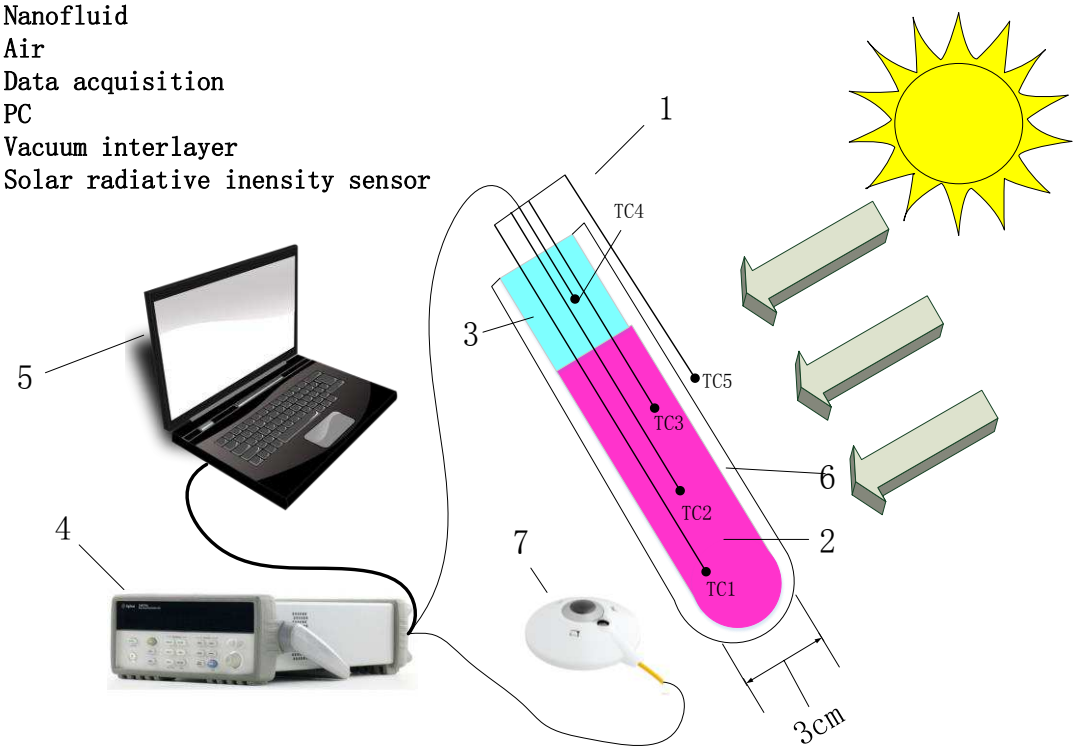

Fig. 2. Experimental setup: (a) Soar thermal illumination experiment under natural sunlight conditions (location 39° 59' 5.49" North, 116° 21' 18.70" East.) and (b) A schematic illustration of the experimental setup.

(a)

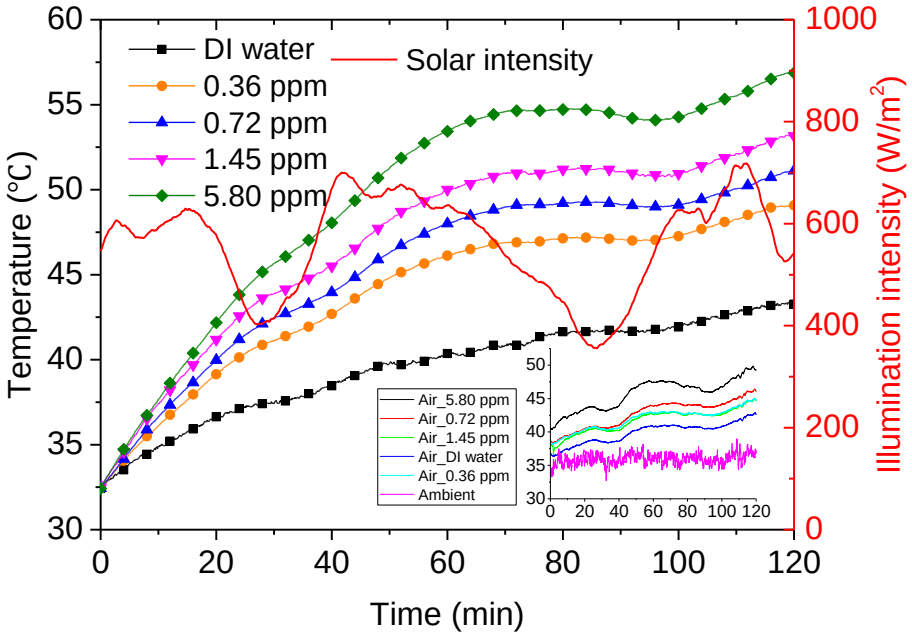
DI water
0.36 ppm
0.72 ppm
1.45 ppm
5.80 ppm
Solar intensity
Temperature (°C)
Illumination intensity (W/m²)
Time (min)
Air_5.80 ppm
Air_0.72 ppm
Air_1.45 ppm
Air_DI water
Air_0.36 ppm
Ambient

560

(b)

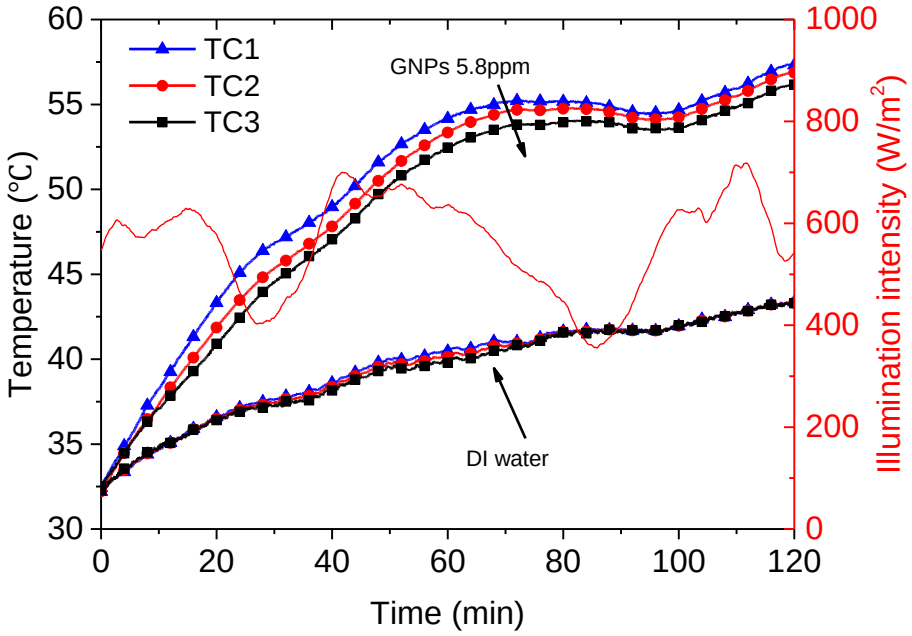
TC1
TC2
TC3
GNPs 5.8ppm
DI water
Temperature (°C)
Illumination intensity (W/m²)
Time (min)

561

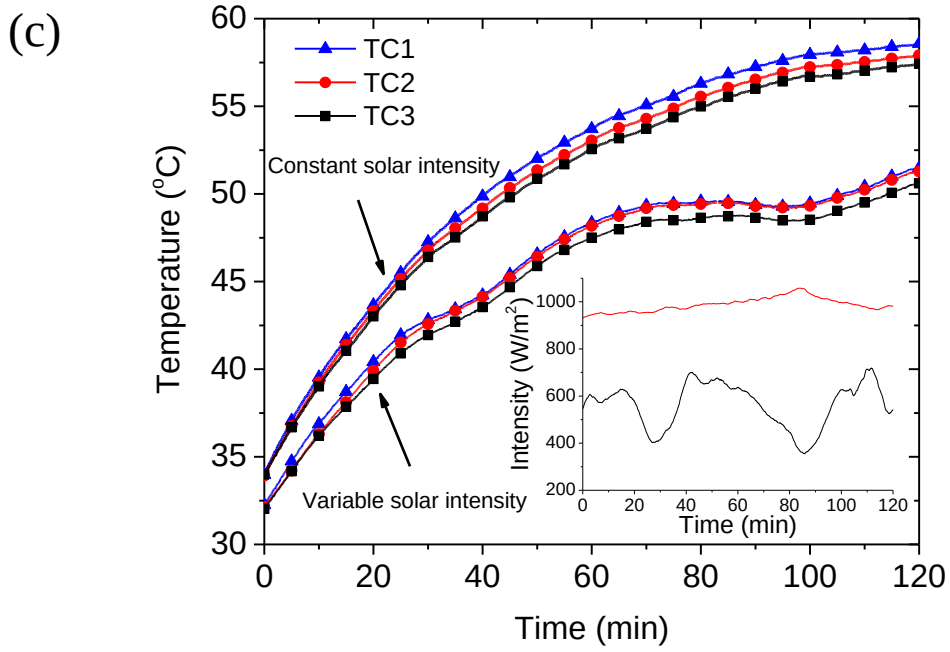

562

563

564 **Fig. 3.** (a) Example temperature profile of differentnanofluids under a cloudy day (solar intensity varied from about 400 W/m^2 to

565 700 W/m^2); (b) Temperature profile of TC1-TC3 located inside the fluid for 5.8 ppm nanofluids in the cloudy day. (c)

566 Comparison of three thermocouple profiles for 0.72 ppm gold nanofluid under different solar intensities: constant solar

567 intensity (i.e., about 950 W/m^2) and varied solar intensity (i.e., from 400 W/m^2 to 700 W/m^2).

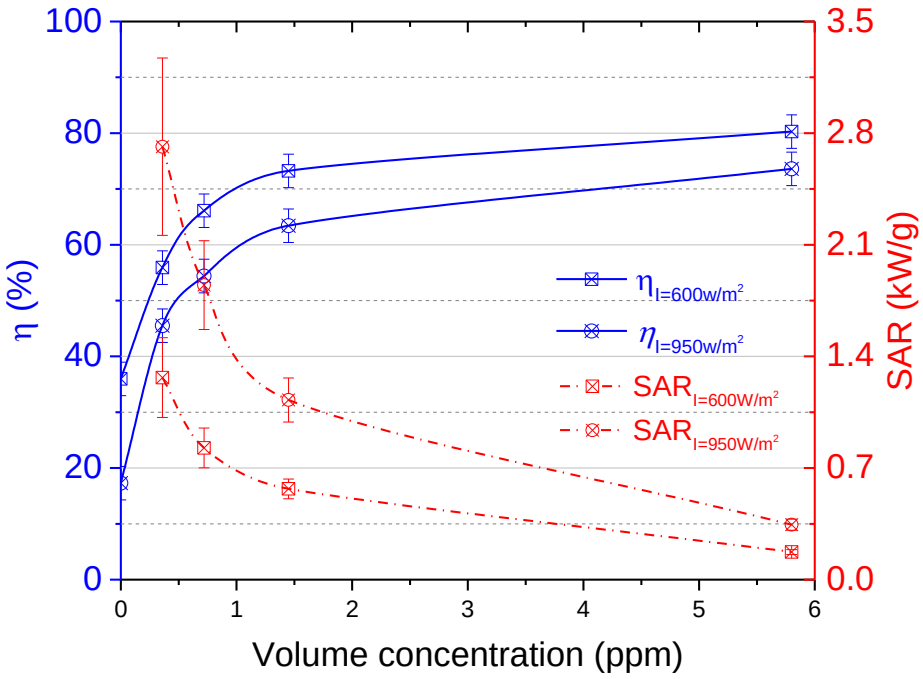

568

569 **Fig. 4.** Variation of photothermal conversion efficiency (η) and specific absorption rate （SAR）with volume concentration of

570 gold nanofulids under different solar intensities.

571

572

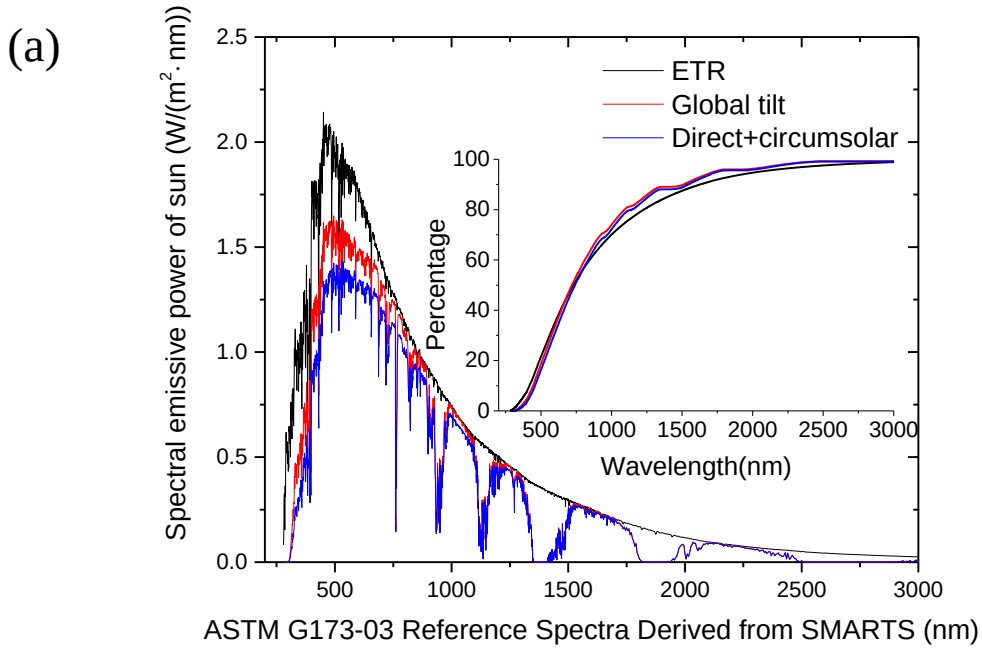

573

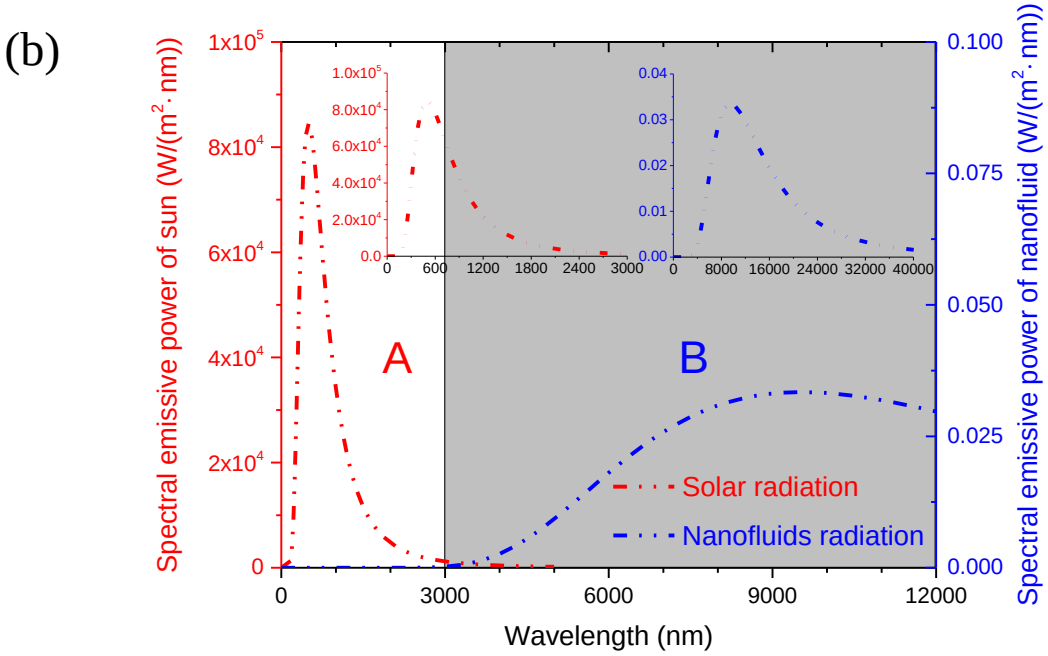

574

575 **Fig. 5.** (a) ASTM G173-03 Reference Spectra from literature, inset shows the solar energy distribution along with wavelength in

576 percentage (integrating spectral emissive power with wavelength divided by irradiation intensity). (b) Calculation of spectral

577 emissive power for sun (T=5762 K) and nanofluid (T=303 K), where spectral distribution is separated into two bands, **A**

578 (λ<3000 nm) and **B** (λ > 3000 nm).

(a)

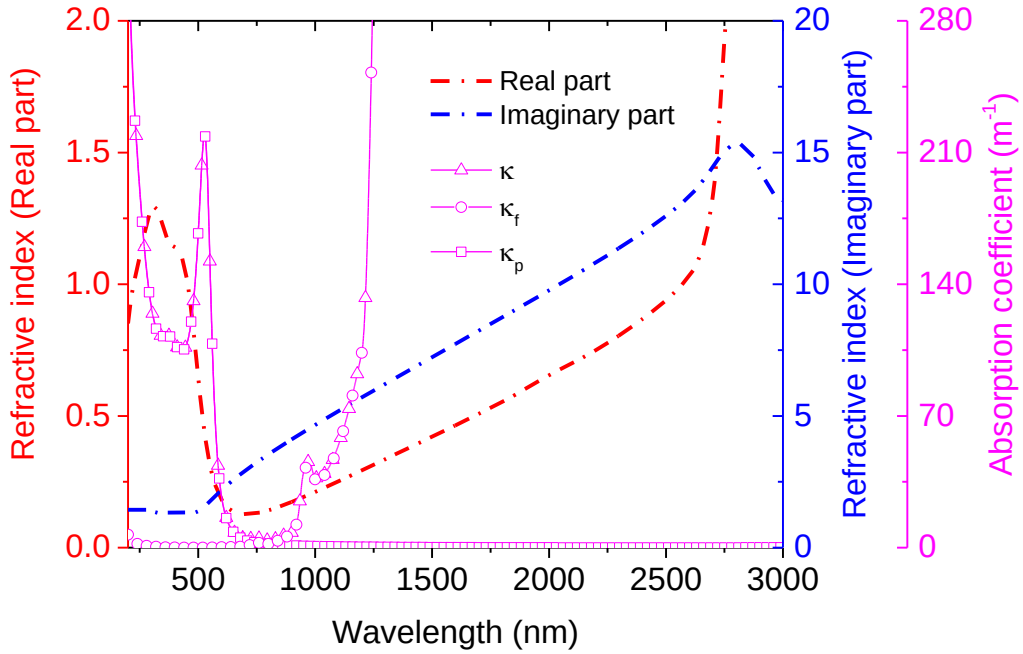

579

(b)

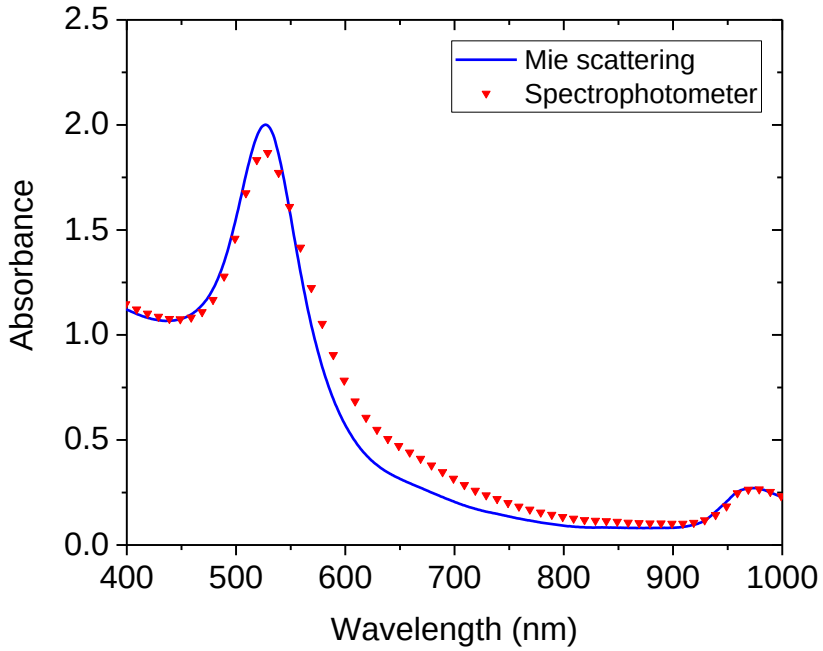

580

581 **Fig.6.** (a) Real and imaginary parts of m (Eq. (2)) and calculated absorption coefficients for gold nanoparticles (κ_p), working

582 fluid (κ_f) and total (κ) according to Mie scattering theory; (b) Absorbance from Eq. (10) in comparison with the results from

583 the UV spectrophotometer.

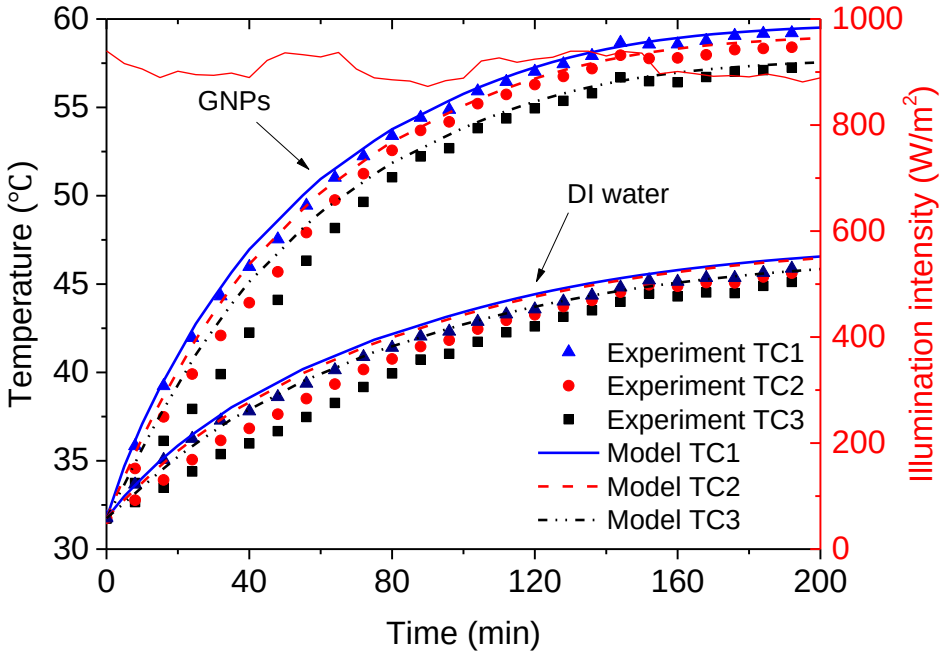

584

585 **Fig. 7.** Comparions between experimentally obtained increasing temperature profile of TC1-TC3 with numerical results from 3D

586 model (nanofluids concentration is 1.45 ppm and solar intensity is constantly ~ 950 W/m^2)

(a)

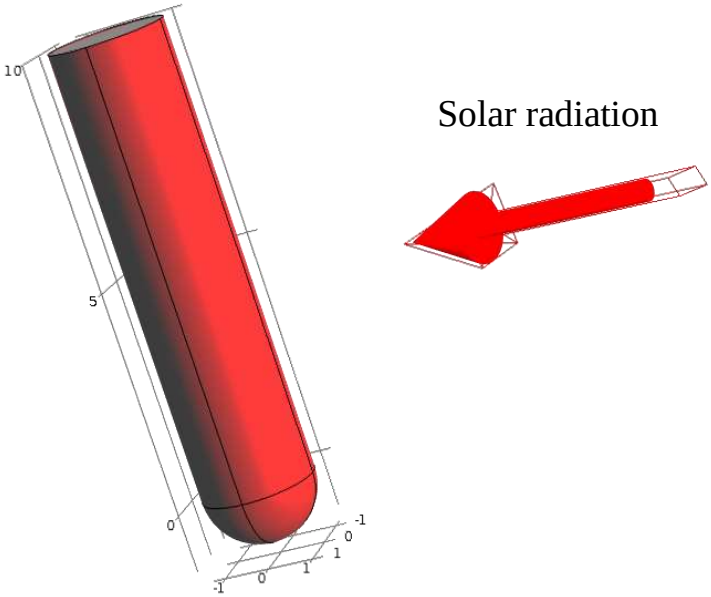

587

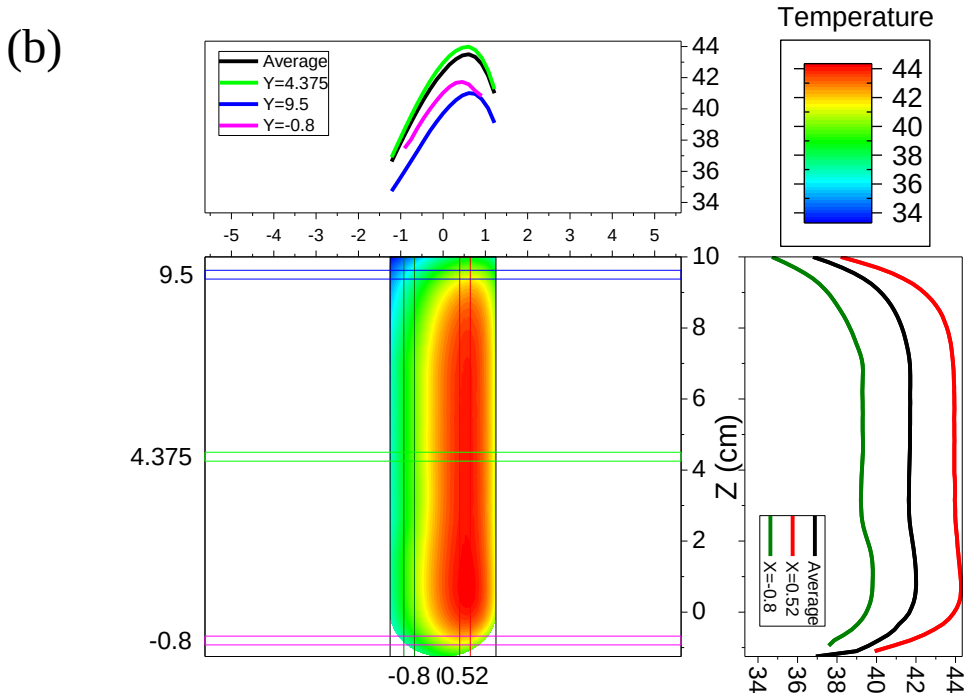

588

589

590 **Fig. 8.** (a) Schematic illustration of numerical simulation of a 3-D volumetric solar receiver where the geometry parameters is

591 shown in (b) and solar radiation is in -y direction; (b) Temperature contour and cross-sectional profiles for nanofluid after 30

592 minutes' illumination (Global Tilt, x=0 cm, gold nanofluid concentration =1.45 ppm, and solar intensity I=900 W/m^2,

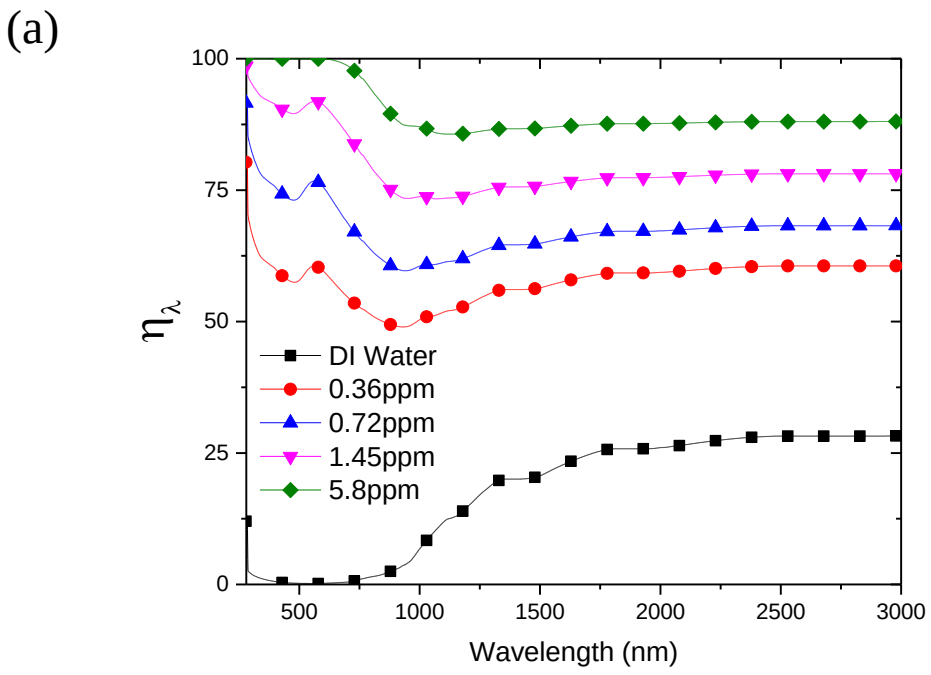

593

(b)

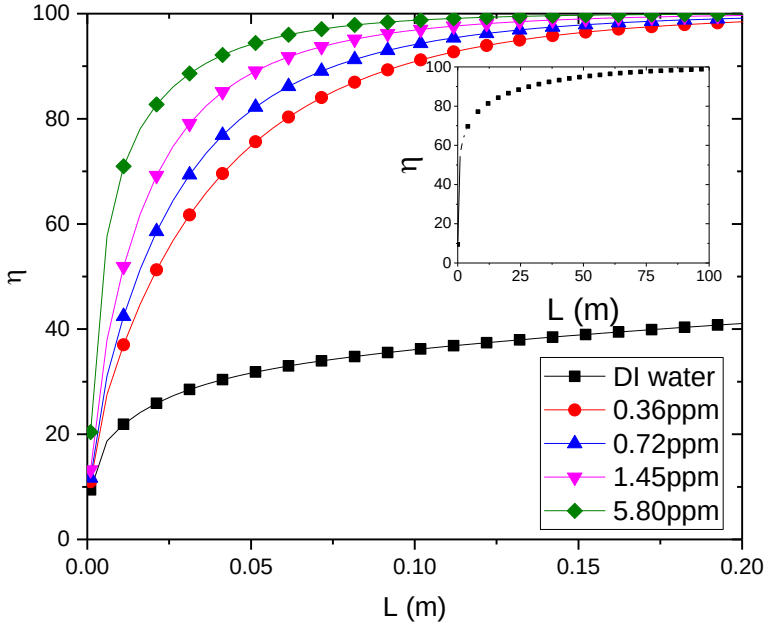

594

(c)

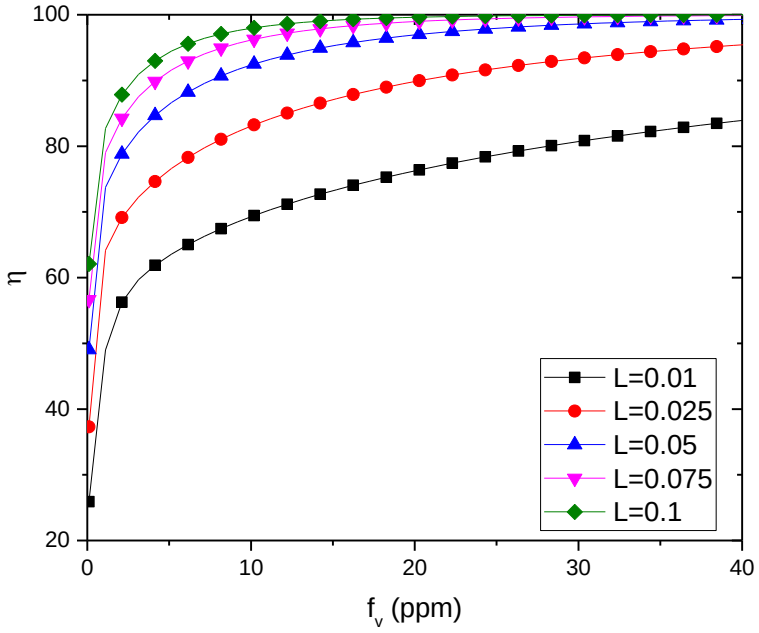

595

596 **Fig. 9.** (a) Spectral absorption efficiency at different wavelength as below in this paper:

597 $\eta_\lambda(\lambda_c)=\left[\int_{0.2\mu m}^{\lambda_c} E_0(\lambda)\left(1-e^{-\kappa(\lambda)L}\right)d\lambda\right]/\left[\int_{0.2\mu m}^{\lambda_c} E_0(\lambda)d\lambda\right]$; (b) Absorption efficiency (ABE) as a function of optical length L for 5

598 different volume concentrations (inset: DI water); (c) ABE as a function of volume concentration f_v for 5 different optical lengths.

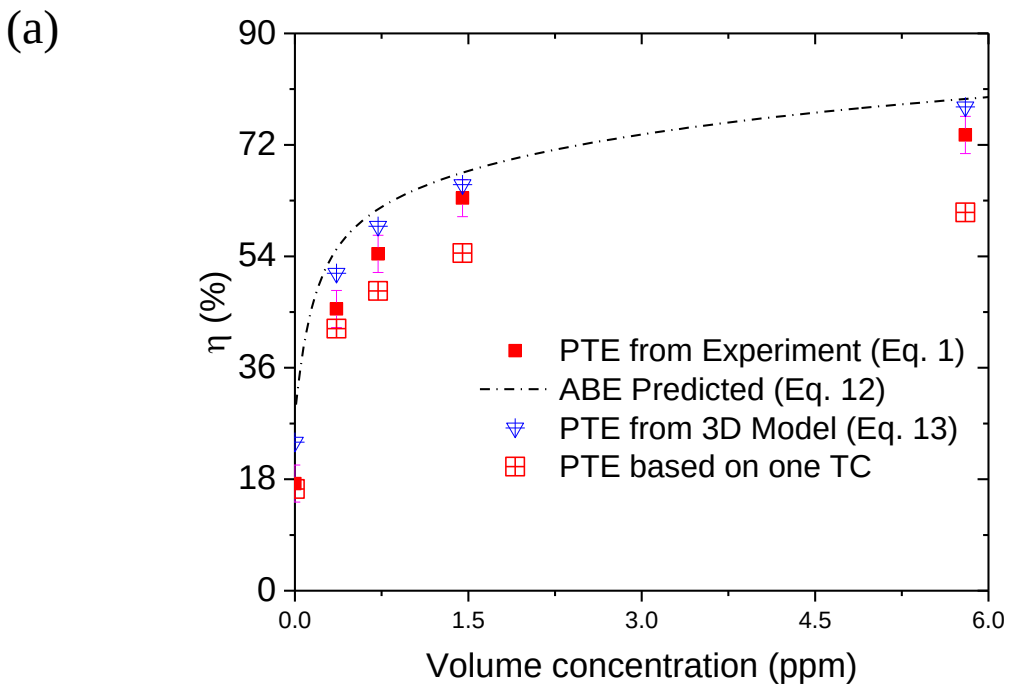

599

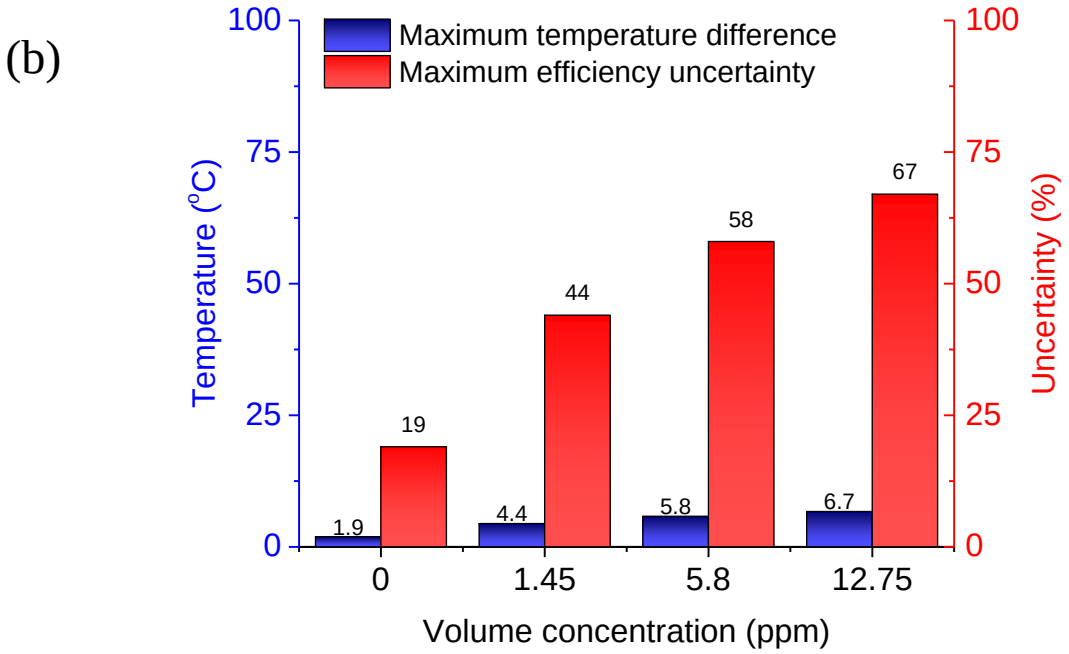

600

601 **Fig. 10.** (a) Comparison of the experimentally obtained photothermal conversion efficiency, efficiency calculated from 3D model
602 and predicted absorption efficiency; (b) Maximum efficiency uncertainty caused by non-uniform temperature distribution in
603 nanofluids.